Mice Carrying a Schizophrenia-associated Mutation of the Arhgap10 Gene Are Vulnerable to the Effects of Methamphetamine Treatment on Cognitive Function: Association With Morphological Abnormalities in Striatal Neurons

Kazuhiro Hada
Nagoya University: Nagoya Daigaku https://orcid.org/0000-0002-7742-0068
Bolati Wulaer
Nagoya University: Nagoya Daigaku
Taku Nagai
Nagoya University: Nagoya Daigaku
Norimichi Itoh
Nagoya University: Nagoya Daigaku
Masahito Sawahata
Nagoya University: Nagoya Daigaku
Akira Sobue
Nagoya University: Nagoya Daigaku
Hiroyuki Mizoguchi
Nagoya University: Nagoya Daigaku
Daisuke Mori
Nagoya University: Nagoya Daigaku
Itaru Kushima
Nagoya University: Nagoya Daigaku
Toshitaka Nabeshima
Fujita Health University: Fujita Ika Daigaku
Norio Ozaki
Nagoya University: Nagoya Daigaku
Kiyofumi Yamada (kyamada@med.nagoya-u.ac.jp)
Department of Neuropsychopharmacology and Hospital Pharmacy, Nagoya University 9 Graduate School of Medicine, Nagoya 466-8560, Japan

Research

Keywords: ARHGAP10, schizophrenia, methamphetamine, spine, Visual discrimination

Posted Date: October 22nd, 2020

DOI: https://doi.org/10.21203/rs.3.rs-94489/v1

Version of Record: A version of this preprint was published on January 22nd, 2021. See the published version at https://doi.org/10.1186/s13041-021-00735-4.

Mice carrying a schizophrenia-associated mutation of the *Arhgap10* gene are vulnerable to the effects of methamphetamine treatment on cognitive function: association with morphological abnormalities in striatal neurons

Kazuhiro Hada[1, #], Bolati Wulaer[1, 2, #], Taku Nagai[1, 3, #], Norimichi Itoh[1], Masahito Sawahata[1], Akira Sobue[1], Hiroyuki Mizoguchi[1], Daisuke Mori[4, 6], Itaru Kushima[4, 7], Toshitaka Nabeshima[2, 5], Norio Ozaki[4, 6, 7], Kiyofumi Yamada[1, 5, *]

[1]Department of Neuropsychopharmacology and Hospital Pharmacy, Nagoya University Graduate School of Medicine, Nagoya 466-8560, Japan

[2]Advanced Diagnostic System Research Laboratory, Fujita Health University Graduate School of Health Science, Aichi 470-1192, Japan

[3]Project Office for Neuropsychological Research Center, Fujita Health University, Aichi 470-1192, Japan

[4]Department of Psychiatry, Nagoya University Graduate School of Medicine, Nagoya 466-8560, Japan

[5]Japanese Drug Organization of Appropriate Use and Research, Aichi, Japan

[6]Brain and Mind Research Center, Nagoya University, Nagoya, Aichi, Japan

[7]Medical Genomics Center, Nagoya University Hospital, Nagoya, 466-8560, Japan.

E-mail address

Kazuhiro Hada: kazuhiro-888@med.nagoya-u.ac.jp

Bolati Wulaer: ularb@fujita-hu.ac.jp

Taku Nagai: taku.nagai@fujita-hu.ac.jp

Norimichi Itoh: n-ito@med.nagoya-u.ac.jp

Masahito Sawahata: m-sawahata@med.nagoya-u.ac.jp

Akira Sobue: a-sobue@riem.nagoya-u.ac.jp

Hiroyuki Mizoguchi: hmizoguchi@med.nagoya-u.ac.jp

Daisuke Mori: d-mori@med.nagoya-u.ac.jp

Itaru Kushima: kushima@med.nagoya-u.ac.jp

Toshitaka Nabeshima: tnabeshi@fujita-hu.ac.jp

Norio Ozaki: ozaki-n@med.nagoya-u.ac.jp

Kiyofumi Yamada: kyamada@med.nagoya-u.ac.jp

[#]Co-first authors: Kazuhiro Hada, Bolati Wulaer and Taku Nagai

[*]Correspondence to: Kiyofumi Yamada, Ph.D., Department of Neuropsychopharmacology and Hospital Pharmacy, Nagoya University Graduate School of Medicine, 65 Tsurumai, Showa, Nagoya 466-8560, Aichi, Japan.

Tel.: +81-52-744-2674; Fax: +81-52-744-2979

E-mail address: kyamada@med.nagoya-u.ac.jp

Page count: 37

Abstract word count: 248

Introduction word count: 496

Discussion word count: 1022

Abstract

We recently found a significant association between exonic copy-number variations in the Rho GTPase activating protein 10 (*Arhgap10*) gene and schizophrenia in Japanese patients. Special attention was paid to one patient carrying a missense variant (p.S490P) in exon 17, which overlapped with an exonic deletion in the other allele, because two mutations in the same gene are considered a typical genetic model of severe schizophrenia. Accordingly, we generated a mouse model (ARHGAP10$^{NHEJ/S490P}$ mice) carrying a missense variant and a coexisting frameshift mutation (NHEJ). We examined the spatiotemporal expression of *Arhgap10* mRNA in the brain and found the highest expression levels in the striatum and nucleus accumbens (NAc), followed by the frontal cortex in adolescent mice. The expression levels of phosphorylated myosin phosphatase-targeting subunit 1 and phosphorylated p21-activated kinases in the striatum and NAc were significantly increased in ARHGAP10$^{NHEJ/S490P}$ mice compared with WT littermates. ARHGAP10$^{NHEJ/S490P}$ mice exhibited a significant increase in neuronal complexity and spine density in the striatum and NAc. There was no difference in touchscreen-based visual discrimination (VD) learning between ARHGAP10$^{NHEJ/S490P}$ and WT mice, but a significant impairment of VD was evident in ARHGAP10$^{NHEJ/S490P}$ mice but not WT mice when they were treated with methamphetamine. The number of c-Fos-positive cells was significantly increased after methamphetamine treatment in the dorsomedial striatum and NAc core of ARHGAP10$^{NHEJ/S490P}$ mice. Taken together, these results suggested that schizophrenia-associated *Arhgap10* gene mutations result in morphological abnormality in the striatum and NAc neurons, which may be associated with vulnerability of cognition to methamphetamine treatment.

69

70 Keywords: ARHGAP10; schizophrenia; methamphetamine; spine; Visual discrimination

Introduction

Schizophrenia (SCZ) is a highly debilitating mental disorder that affects about 1% of the overall population. Although the pathoetiology in SCZ remains to be determined [1], both genetic and environmental factors are involved in developmental abnormalities in the brains of patients [2, 3]. Several environmental factors have been reported as risk factors for SCZ, namely maternal virus infection, malnutrition, and juvenile cannabis addiction [4-6]. Genomic studies have also suggested a role for rare copy-number variations (CNVs), defined as copy number changes including deletions and duplications of genomic regions in SCZ. Rare CNVs in specific loci have been identified as risk factors for SCZ, including deletions at 1q21.1, NRXN1, 3q29, 15q11.2, 15q13.3, and 22q11.2 and duplications at 1q21.1, 7q11.23, 15q11.2-q13.1, 16p13.1, and 16p11.2 [7-12].

We recently performed CNV analysis in Japanese SCZ patients and control-subjects and identified a significant association between SCZ and exonic CNVs in the Rho GTPase activating protein 10 (*Arhgap10*) gene. Exonic CNVs in ARHGAP10 were identified in 7 patients (six cases with deletions and one with duplication), but not in control subjects [13]. ARHGAP10, a member of the Rho GTPase activating proteins (GAPs), inactivates RhoA and Cdc42 by converting the GTP-bound form to the GDP-bound form [14, 15]. Among 7 patients with exonic CNVs, one patient (Case #5) had a missense variant (p.S490P) in exon 17, which overlapped with an exonic deletion on the other allele and was located in the RhoGAP domain, leading to the activation of RhoA signaling. The patient had poor premorbid functioning (e.g., poor academic performance and social skills) prior to the onset of SCZ [13]. Two mutations in the same gene, such as in Case #5, have been proposed to represent a typical genetic model of severe SCZ [16]. Accordingly, we generated mice with variants of *Arhgap10* that mimicked the Case #5

genotype. The model mice, ARHGAP10$^{NHEJ/S490P}$ mice, carrying a missense variant (p.S490P) and a coexisting frameshift mutation caused by non-homologous end-joining (NHEJ) showed an increase in anxiety-related behavior in the elevated plus-maze test and a hypersensitivity to methamphetamine (METH) in the locomotor test [13].

To elucidate the relationship between mutations in the *Arhgap10* gene and the clinical symptoms of SCZ, pathophysiological, morphological, and behavioral phenotypes were investigated in ARHGAP10$^{NHEJ/S490P}$ mice. Previous studies indicated the morphological abnormality of pyramidal neurons in the prefrontal cortex of patients with SCZ [17-19], whereas ARHGAP10 is reported to regulate cellular morphology through the RhoA and Cdc42 pathways in fibroblasts [20]. Thus, we analyzed neuronal morphology and spine density in ARHGAP10$^{NHEJ/S490P}$ mice. Moreover, SCZ patients exhibit cognitive dysfunction and abnormal drug reactivity: amphetamine (AMPH) administration at small doses can produce or enhance a psychotic reaction in patients with SCZ, but not in healthy controls [21, 22]. Similarly, ARHGAP10$^{NHEJ/S490P}$ mice showed a higher sensitivity to METH in the locomotor test [13]. Therefore, cognitive function and vulnerability to METH in ARHGAP10$^{NHEJ/S490P}$ mice were further evaluated using a touchscreen-based visual discrimination (VD) task that can evaluate higher brain functions in mice with high translational validity.

Materials and Methods

Animals

ARHGAP10$^{NHEJ/S490P}$ mutant mice (NHEJ and S490P line) were generated in a C57BL/6J genetic background as described previously [13]. ARHGAP10$^{NHEJ/S490P}$ (n = 29) mice and their wild-type (WT) littermates (n = 50) were obtained by breading two lines of heterozygous

ARHGAP10 mutant mice (NHEJ line and S490P line). Male mice were used in the experiment because some behavioral abnormalities have been observed in male but not female mice [13]. Mice were housed at a density of 5–6 mice per cage (28 cm length × 17 cm width × 13 cm high) in standard conditions (23 ± 1°C, 50 ± 5% humidity) with a 12-h light/dark cycle. Food and water were available ad libitum.

RNA extraction and reverse transcription quantitative real-time polymerase chain reaction

Reverse transcription quantitative real-time polymerase chain reaction (RT-qPCR) was performed as described previously [23]. Tissues were quickly dissected out on ice, and total RNA was extracted using a RNeasy Mini Kit (Cat# 74106, QIAGEN, Hilden, Germany). Total RNA was reverse transcribed using the SuperScript III First-Strand Synthesis System for RT-PCR (Cat# 18080-051, Invitrogen, Carlsbad, CA), and determined by real-time PCR using an ABI PRISM 7300 real-time PCR system (Thermo Fisher Scientific, Yokohama, Japan). The primers used in the present study were as follows: *Arhgap10* (Cat# QT00278684, QIAGEN), *Gapdh* forward, CAATGTGTCCGTCGTGGATCT; *Gapdh* reverse, GTCCTC AGTGTAGCCCAAGATG.

***In situ* hybridization**

The probe for *in situ* hybridization (ISH) analysis was designed from positions 1216–1571 of the *Arhgap10* genomic DNA (GenBank accession number: NM_030113.2). Dissected mouse brain at the age of 8 weeks old was fixed with G-Fix (Cat# STF-02, Genostaff, Tokyo, Japan) and embedded in paraffin on CT-Pro20 (Genostaff) using G-Nox (Cat# GN04, Genostaff). ISH was performed using an ISH Reagent Kit (Cat# SRK-02, Genostaff) in accordance with the

manufacturer's instructions. Briefly, de-paraffinized and rehydrated brain slices (8 μm) were fixed with 10% neutral buffered formalin (NBF) for 15 min at room temperature (RT) followed by treatment with proteinase K (Cat# 164-14004, 4 mg/ml; Wako Pure Chemical Industries, Ltd, Osaka, Japan) in phosphate-buffered saline (PBS) for 10 min at 37°C. After washing in PBS, samples were re-fixed with 10% NBF for 15 min at RT and placed in 0.2 M HCl for 10 min at RT. The PBS-washed sample was placed in a coplin jar containing 1×G-Wash (Cat# SHW-01, Genostaff). Hybridization was performed with probes at concentrations of 300 ng/ml in G-Hybo-L/G-Hybo (Cat# RPD-02 and RPD-01, respectively; Genostaff) for 16 hrs at 60°C. After hybridization, the sections were washed in 1×G-Wash for 10 min at 60°C, and 50% formamide in 1×G-Wash for 10 min at 60°C. Then, the sections were washed twice in 1×G-Wash for 10 min at 60°C, and twice in 0.1×G-Wash for 10 min at 60°C, and twice in 0.1% Tween 20 in Tris-buffered saline (TBS) at RT. After treatment with 1×G-Block (Cat# GB-01, Genostaff) for 15 min at RT, the sections were incubated with anti-digoxigenin alkaline phosphatase conjugate (Cat# 11093274910, Roche, Diagnostics GmbH, Mannheim, Germany) diluted 1:2000 with G-Block in 0.1% Tween 20 in TBS for 1 hr at RT. The sections were incubated in 100 mM NaCl, 50 mM $MgCl_2$, 0.1% Tween 20, 100 mM Tris-HCl, pH 9.5. Coloring reactions were performed with 5-bromo-4-chloro-3-indolyl-phosphate/nitroblue tetrazolium solution (Cat# B6149, Cat# 34035, respectively; Sigma-Aldrich, MO, USA) overnight and then washed in PBS. The sections were counterstained with Kernechtrot stain solution (Cat# 40871, Muto Pure Chemicals, Tokyo, Japan), and mounted with G-Mount (Cat# GM-01, Genostaff).

Western blotting

Western blotting was performed as described previously [24]. In brief, the striatum (ST) and nucleus accumbens (NAc) tissue were sonicated and boiled at 99°C in lysis buffer [complete protease inhibitor cocktail (Cat# 11873580001, Roche) for 10 min, and phosSTOP phosphatase inhibitors (Cat# 4906837001, Roche) in 1% SDS solution]. Samples were centrifuged at 15,000 rpm for 20 min. The protein concentration was determined using a DC Protein Assay Kit (Cat# 5000111JA, Bio-Rad Laboratories, Hercules, CA), and protein was boiled in sample buffer (0.5 M Tris-HCl, pH 6.8, 1% SDS, 30% glycerol, 0.0012% bromophenol blue, and 0.93% DTT); applied to an 8% SDS-polyacrylamide gel; and subsequently transferred to a polyvinylidene difluoride membrane (Cat# IPVH00010, Millipore, Darmstadt, Germany). The membranes were blocked with Blocking One-P (Cat# 05999-84, Nacalai Tesque, Kyoto, Japan) at RT for 1 hr and incubated with a primary antibody at 4°C overnight. Then, membranes were washed three times every 10 min with 1% Tween 20 in TBS. After incubation with horseradish peroxidase (HRP)-conjugated secondary antibody at RT for 1 hr, the immune complex was detected using ECL Plus Western blotting detection reagents (Cat# RPN2236, GE Healthcare, Pittsburg, PA, USA). The intensities of the bands on the membranes were analyzed using a LuminoGraph I (Atto Instruments, Tokyo, Japan). To calculate the relative amount of phosphorylated proteins compared with total proteins, the same membranes were stripped with WB Stripping Solution Strong (Cat# 05677-65, Nacalai Tesque) at RT for 1 hr and treated as described above. Because there was no change in the levels of total proteins, values of phosphorylation were normalized to the values of total proteins. All the data from western blotting were expressed as relative fold change in expression relative to the control. The primary and secondary antibodies were diluted with Can Get Signal Solution 1 and 2 (Cat# NKB-101, Toyobo Co., Ltd, Osaka, Japan), respectively, to enhance antibody-antigen binding. The primary antibodies were used as follows:

a rabbit anti-myosin phosphatase-targeting subunit 1 (MYPT1) (Cat# 2634, RRID:AB_915965, 1:1,000; Cell Signaling Technology, Danvers, MA), and rabbit anti-phospho-MYPT1 (Thr696) (Cat# ABS45, RRID:AB_10562238, 1:1,000; Millipore), rabbit anti-p21-activated kinase (PAK) 1/2/3 (Cat# 2604, RRID:AB_2160225, 1:500; Cell Signaling Technology), rabbit anti-phospho-PAK1 (Ser144) /PAK2 (Ser141) (Cat# 2606, RRID:AB_2299279, 1:1,000; Cell Signaling Technology). The secondary antibodies were HRP-conjugated anti-rabbit IgG antibody (Cat# NA9340, RRID:AB_772191, 1:10,000; GE Healthcare).

In vivo microdialysis

In vivo dialysis was performed as described previously [25]. Mice were anesthetized with tribromoethanol (250 mg/kg, intraperitoneal administration (i.p.)) and a guide cannula (AG-6; Cat# 801224, Eicom Corp., Kyoto, Japan) was implanted in the NAc (+1.5 mm anteroposterior, +0.8 mm mediolateral from the bregma, and 4.0 mm dorsoventral from the skull) according to the mouse brain atlas (Franklin and Paxinos, 1997). Two days after recovery from surgery, a dialysis probe (A-I-6-01; Cat# 801026, membrane length of 1 mm, Eicom Corp.) was inserted through the guide cannula and perfused with artificial cerebrospinal fluid (aCSF; 147 mM NaCl, 4 mM KCl, and 2.3 mM $CaCl_2$) at a flow rate of 1.0 μl/min. Outflow fractions were collected every 5 min. After the collection of baseline fractions, mice were treated with METH (1.0 mg/kg, i.p.). Dopamine (DA) levels in the dialysates were analyzed using a high-performance liquid chromatography system (HTEC-500, Eicom Corp.) equipped with an electrochemical detector.

c-Fos immunohistochemistry

The details of the procedure were described in a previous report [26]. Briefly, animals were deeply anesthetized with tribromoethanol (250 mg/kg, i.p.) and perfused transcardially with 0.1 M phosphate buffer (PB) followed by 4% paraformaldehyde (PFA) solution. The brain was removed and fixed overnight in 4% PFA and stored in 30% sucrose, embedded in Tissue-Tek O.C.T. compound (Cat# 4583, Sakura Finetech, Tokyo, Japan), and then stored at -80 ˚C. Brain areas were determined according to the mouse brain atlas. Brain slices (30 µm thickness) were washed with PBS containing 0.3% Triton X-100 and blocked at RT for 2 hrs in a presence of 2% normal goat serum (Cat# S-1000, Vector Laboratories Inc, Burlingame CA, USA). The samples were incubated with rabbit anti-c-Fos antibody (Cat# PC38, RRID:AB_2106755, 1:10,000; EMD Millipore, Billerica, Massachusetts, USA) at 4°C overnight. After washing with PBS, the sections were incubated with a biotinylated goat anti-rabbit IgG secondary antibody (Cat# BA-1000, RRID:AB_2313606, 1:1,000, Vector Laboratories Inc) at RT for 2 hrs. The sections were then incubated with PBS containing 0.3% hydrogen peroxide for 30 min, and treated with avidin-biotinylated horseradish peroxidase complex (Vectastain ABC kit; Cat# PK-6100, Vector Laboratories Inc) at RT for 2 hrs. Signals were visualized using the diaminobenzidine–nickel method. The number of c-Fos-positive cells was measured within a region of interest (340 µm × 460 µm sized area) using Metamorph software (Molecular Devices, Sunnyvale, CA, USA). Nine regions of interest from three mice were used in each group.

Golgi staining and morphological analysis

Golgi staining was performed using a FD Rapid Golgi Stain Kit (Cat# PK401, FD NeuroTechnologies, Ellicott City, MD) as described previously [23]. Neurolucida software (MicroBrightField Bioscience, Williston, VT) was used to trace neurons on BZ9000 bright-field

microscopic (KEYENCE, Osaka, Japan) images (at 100×magnification). Neurons were analyzed in the ST and NAc. All of the neurons analyzed were well stained and isolated and had intact dendritic arbors. Node numbers, intersections, dendritic length, and ending numbers of each traced neuron were analyzed using NeuroExplorer software (MicroBrightField Inc). Four mice were used in each group. Two to three neurons were traced per mice.

Dendritic spines were counted in secondary dendrites of neurons on branches. According to their morphology in previous reports [27], protrusions were distinguished into four categories; (1) mushroom spines with a large head (width >0.6 μm); (2) stubby spines with a head but without a neck; (3) thin spines with a long neck (length >1 μm) and small heads; and (4) branch spines with more than two heads. The number of spines was measured from 4 different secondary dendrites per mouse. Four mice were used in each group.

Touchscreen-based VD task

The protocol was described in previous reports [26, 28]. Briefly, mice were restricted in their access to food and water for 2 hrs (5 pm–7 pm) on a day at least 1 week before the pretraining to provide enough motivation to perform the task. The food and water restriction was continued until the end of the task. The task started with 5 stages pretraining (habituation, initial touch, must touch, must initiate, and punish incorrect) to shape screen-touching behavior in the mice. After mice completed this pretraining (>75% for 2 consecutive days), they were subsequently moved to the VD task. In the VD task, trial initiation was triggered by mice touching the nozzle, and 2 stimuli (marble and fan) were then presented simultaneously in the 2 response windows. Touching the correct window resulted in the delivery of a liquid reward (20 μl). When the incorrect window was touched, the stimuli offset immediately and a 5 s time-out period was

started. After an inter-trial interval (20 sec), a correction trial was given instead of a new trial. In the correction trial, the same stimulus set was repeatedly presented in the same location until the mouse made a correct response. Stimulus contingencies were counterbalanced. The session finished after 1 hr or 30 trials were completed, whichever came first. The total number of trials, total number of correction trials, response latencies, percentage of trials completed, and correction errors, as well as the percentage of correct responses, were analyzed.

When mice could perform with more than 80% correct responses for 2 consecutive days, the reversal learning task was begun, this stage was similar to the initial acquisition of the VD task, except that the contingency of the stimulus pair was reversed.

Drug treatment

METH (Sumitomo Dainippon Pharma, Osaka, Japan) or saline was administered i.p. to mice 2 hrs before immunohistochemistry. In behavioral analyses, mice were treated with METH (0.1 ml/10 g body weight) 30 mins before the start of the VD test.

Statistical analyses

All data are expressed as means±SEM. Statistical significance was determined using Mann–Whitney U-test for comparisons of two groups. For multiple comparisons, statistical significance was determined using an analysis of variance (ANOVA) with repeated measures, and Tukey–Kramer test was used for post-hoc analysis when F ratios were significant.

Results

Spatiotemporal expression of *Arhgap10* mRNA in the mouse brain

Arhgap10 is expressed in the brain [15, 20], and it plays an important role in the development of the brain [13, 29]. On the other hand, SCZ is considered a neurodevelopmental disorder and patients have anatomical and functional abnormalities in the frontal cortex (Fc) and the hippocampus (Hip) [30-34]. Therefore, developmental changes in the levels of *Arhgap10* mRNA expression were investigated in the Hip and Fc of naïve C57BL/6J mice from embryonic day (E) 14 to postnatal day (P) 56 by RT-qPCR. The relative level of *Arhgap10* mRNA in the Hip and Fc increased in an age-dependent manner, and a significant increase in *Arhgap10* mRNA levels was detected at P56 compared with P0 (Hip; $F_{(5, 12)} = 25.9$, $p < 0.01$, Fc; $F_{(5, 12)} = 111.8$, $p < 0.01$, one-way ANOVA, **Fig. 1a**). At P56, *Arhgap10* mRNA expression was compared with various brain regions including the ST, NAc, substantia nigra/ventral tegmental area (SN/VTA), and raphe nuclei (Rn). The highest expression levels of *Arhgap10* mRNA were observed in the ST and NAc, followed by the Fc. The expression levels in other brain regions such as the Hip, SN/VTA, and Rn were low (brain region, $F_{(5, 12)} = 54.6$, $p < 0.01$, one-way ANOVA, **Fig. 1b**). The signal of *Arhgap10* mRNA was also detected in the ST and Fc by ISH (**Fig. 1c, d**). Taken together, *Arhgap10* mRNA expression increased in an age-dependent manner in the mouse brain, in which the ST and NAc exhibited the highest expression levels in measured brain regions during adolescence.

Activation of MYPT1 and PAKs in the ST and NAc of ARHGAP10$^{NHEJ/S490P}$ mice

Rho-kinase (ROCK) is a downstream effector of RhoA [35], whereas PAKs act as the downstream effectors for Cdc42 and Rac1 [36]. ROCK phosphorylates MYPT1 at Thr696, resulting in a decrease in myosin light chain (MLC) phosphatase activity and an increase in phosphorylated MLC [35]. Accordingly, the effect of *Arhgap10* gene mutations on the

299 downstream signal activity was investigated using phospho-MYPT1 and phospho-PAK1/2 levels
300 in the ST and NAc of ARHGAP10$^{NHEJ/S490P}$ mice. The phospho-MYPT1 levels were increased in
301 the ST and NAc of ARHGAP10$^{NHEJ/S490P}$ mice compared with WT littermates (ST; $p < 0.01$,
302 NAc; $p < 0.05$, Mann-Whitney U-test, **Fig. 2a-c**). The phospho-PAK1/2 (Ser144/141) levels
303 were also higher in the ST and NAc of ARHGAP10$^{NHEJ/S490P}$ mice than those in WT littermates
304 (ST; $p < 0.01$, NAc; $p < 0.05$, Mann-Whitney U-test, **Fig. 2d-f**). These results suggested that
305 ARHGAP10$^{NHEJ/S490P}$ mice have an abnormality in the Rho signaling pathway in the ST and NAc.
306
307 **Abnormal neuronal morphology in the ST and NAc of ARHGAP10$^{NHEJ/S490P}$ mice**
308 It is well known that RhoA and Cdc42 signaling is involved in the regulation of neuronal
309 morphology [37]. To test the possible changes in neuronal morphology in the ST and NAc of
310 ARHGAP10$^{NHEJ/S490P}$ mice, the brains were subjected to Golgi staining (Fig. **3**). Branching
311 density and complexity of the neurons were assessed using a Sholl analysis method. The analysis
312 revealed abnormal increases in intersections (genotype, $F_{(1, 196)} = 28.6$, $p < 0.01$, distance, $F_{(6, 196)}$
313 $= 46.6$, $p < 0.01$, genotype×distance interaction, $F_{(6, 196)} = 3.91$, $p < 0.01$, two-way ANOVA, **Fig.**
314 **3a, b**), length (genotype, $F_{(1, 196)} = 36.0$, $p < 0.01$, distance, $F_{(6, 196)} = 55.8$, $p < 0.01$,
315 genotype×distance interaction, $F_{(6, 196)} = 5.16$, $p < 0.01$, two-way ANOVA, **Fig. 3a, c**), nodes
316 (genotype, $F_{(1, 196)} = 9.82$, $p < 0.01$, distance, $F_{(6, 196)} = 23.7$, $p < 0.01$, genotype×distance
317 interaction, $F_{(6, 196)} = 3.25$, $p < 0.01$, two-way ANOVA, **Fig. 3a, d**), and endings (genotype, $F_{(1,}$
318 $_{196)} = 12.1$, $p < 0.01$, distance, $F_{(6, 196)} = 29.8$, $p < 0.01$, genotype×distance interaction, $F_{(6, 196)} =$
319 6.88, $p < 0.01$, two-way ANOVA, **Fig. 3a, e**) in the ST neurons of ARHGAP10$^{NHEJ/S490P}$ mice.
320 Similar results were observed in the NAc neurons of ARHGAP10$^{NHEJ/S490P}$ mice in intersections
321 (genotype, $F_{(1, 98)} = 29.4$, $p < 0.01$, distance, $F_{(6, 98)} = 31.0$, $p < 0.01$, genotype×distance

interaction, $F_{(6, 98)} = 4.51$, $p < 0.01$, two-way ANOVA, **Fig. 3f, g**), length (genotype, $F_{(1, 98)} = 35.8$, $p < 0.01$, distance, $F_{(6, 98)} = 36.5$, $p < 0.01$, genotype×distance interaction, $F_{(6, 98)} = 4.96$, $p < 0.01$, two-way ANOVA, **Fig. 3f, h**), nodes (genotype, $F_{(1, 98)} = 13.4$, $p < 0.01$, distance, $F_{(6, 98)} = 10.4$, $p < 0.01$, genotype×distance interaction, $F_{(6, 98)} = 2.05$, $p = 0.066$, two-way ANOVA, **Fig. 3f, i**), and endings (genotype, $F_{(1, 98)} = 26.7$, $p < 0.01$, distance, $F_{(6, 98)} = 18.1$, $p < 0.01$, genotype×distance interaction, $F_{(6, 98)} = 4.08$, $p < 0.01$, two-way ANOVA, **Fig. 3f, j**). These results suggested that the *Arhgap10* gene mutations led to an abnormal increase in neuronal complexity in neurons of the ST and NAc.

Changes in spine density and morphology in the ST and NAc of ARHGAP10$^{NHEJ/S490P}$ mice

Rho signaling is important for intracellular signaling and actin remodeling [38-40]. Stabilization of the actin cytoskeleton is essential for spine shape and density [39, 41, 42]. Spine cytoskeletal stabilization is altered in multiple cortical areas in SCZ [19]. Therefore, the number of spines on secondary dendrites was counted in ST and NAc neurons in WT and ARHGAP10$^{NHEJ/S490P}$ mice. **Figure 4a** shows representative images of dendrites in the ST and NAc. The spine density was significantly increased in the ST and NAc neurons of ARHGAP10$^{NHEJ/S490P}$ mice compared with WT mice (ST; $p < 0.01$, NAc; $p < 0.01$, Mann-Whitney U-test, **Fig. 4b**).

Dendritic spines are often grouped based on their morphologies [43]. Spines were classified into four types (thin, stubby, branch, and mushroom, **Fig. 4c**). Mushroom spines, defined by their characteristically large head and narrow neck, contain the largest excitatory synapses, whereas thin spines are smaller, lack the large head and thin neck, and contain smaller excitatory synapses [44-46]. The numbers of mushroom-type spines were significantly increased in the ST and NAc of ARHGAP10$^{NHEJ/S490P}$ mice compared with WT mice (ST; $p < 0.01$, NAc; p

345 < 0.01, Mann-Whitney U-test, **Fig. 4d**). However, there were no significant differences in the
346 thin, stubby, and branched types of spines between these two groups of mice (thin type; p =
347 0.122, stubby type; p = 1.21, branched type; p = 0.692, Mann-Whitney U-test, **Fig. 4e-g**). Similar
348 results were observed in the NAc of ARHGAP10$^{NHEJ/S490P}$ mice (thin type; p = 0.386, stubby
349 type; p = 0.792, branched type; p = 0.163, Mann-Whitney U-test, **Fig. 4h-k).** These results
350 suggested that *Arhgap10* gene mutations result in dendritic spine changes in the ST and NAc,
351 which may lead to activity-dependent neuronal dysfunction.
352
353 **Impairment of VD in ARHGAP10$^{NHEJ/S490P}$ mice induced by METH**
354 Normal performance in the VD task depends on intact function of the cortico–striato–thalamic
355 circuitry [47]. We have demonstrated previously that the increased neuronal activity in the ST
356 impairs cognitive function in the VD task [26]. Therefore, using the VD task, the functional
357 consequences of morphological abnormality of neurons in the ST and NAc were evaluated in
358 ARHGAP10$^{NHEJ/S490P}$ mice. Somewhat unexpectedly, no differences were observed in the total
359 number of trials to reach the learning criterion of the VD task (p = 0.884, Mann-Whitney U-test,
360 **Fig. 5b**) as well as reversal learning (**Additional fle 1: figure S1**) between WT and
361 ARHGAP10$^{NHEJ/S490P}$ mice, suggesting that the two groups of mice have comparable ability in
362 the VD learning and reversal learning task.
363 METH has been shown to induce cognitive impairment in the VD task [48]. Furthermore,
364 the METH-induced locomotor response was significantly potentiated in ARHGAP10$^{NHEJ/S490P}$
365 mice compared with WT mice [13]. Therefore, the effect of METH on the performance in
366 ARHGAP10$^{NHEJ/S490P}$ mice was tested using the VD task. METH (0.3 or 1.0 mg/kg) was
367 administered 30 min before the VD test once mice had exhibited stable discrimination

368 performance (more than 80% correct responses) for 2 consecutive days. METH (1.0 mg/kg)
369 significantly reduced the accuracy in the VD test in both WT and ARHGAP10$^{NHEJ/S490P}$ mice. Of
370 note, at a lower dose of 0.3 mg/kg, METH significantly reduced the percentage of correct
371 responses in ARHGAP10$^{NHEJ/S490P}$ mice but not in WT mice (genotype, $F_{(1, 33)} = 1.32$, $p = 0.258$,
372 treatment, $F_{(2, 33)} = 14.75$, $p < 0.01$, genotype×treatment interaction, $F_{(2, 33)} = 5.72$, $p < 0.01$, two-
373 way ANOVA, **Fig. 5c**). The reduction in correct responses was not due to motor dysfunction or
374 motivational change because METH-treated mice in both groups successfully completed the 30
375 trials within 1 hr (**Fig. 5d**), and there were no differences between groups in time to make correct
376 responses (genotype, $F_{(1, 33)} = 0.13$, $p = 0.721$, treatment, $F_{(2, 33)} = 4.82$, $p < 0.05$,
377 genotype×treatment interaction, $F_{(2, 33)} = 0.15$, $p = 0.865$, two-way ANOVA, **Fig. 5e**) and
378 retrieve reward (genotype, $F_{(1, 33)} = 2.84$, $p = 0.101$, treatment, $F_{(2, 33)} = 0.47$, $p = 0.631$,
379 genotype×treatment interaction, $F_{(2, 33)} = 0.19$, $p = 0.828$, two-way ANOVA, **Fig. 5f**). These
380 results suggested that ARHGAP10$^{NHEJ/S490P}$ mice are more vulnerable to METH treatment in
381 terms of cognitive function than WT mice.
382
383 **METH-induced changes in neuronal activity of the dorsal ST and NAc in**
384 **ARHGAP10$^{NHEJ/S490P}$ mice**
385 METH increases DA release in the NAc from the nerve terminal of VTA DA neurons [49]. A
386 recent study indicated that acute AMPH treatment upregulates RhoA activity and dopamine
387 transporter internalization [50]. One possible explanation for the higher sensitivity of
388 ARHGAP10$^{NHEJ/S490P}$ mice to METH-induced cognitive impairment in the VD task as well as
389 METH-induced hyperlocomotion [13], is that METH-induced DA release may be potentiated in
390 ARHGAP10$^{NHEJ/S490P}$ mice compared with WT mice. To test this possibility, the extracellular

391 DA levels in the NAc were measured using an in vivo microdialysis method. As shown in
392 **Additional file 2: figure S2**, no differences in the basal level as well as METH (1.0 mg/kg)-
393 induced DA release were observed between WT and ARHGAP10$^{NHEJ/S490P}$ mice. These findings
394 suggested that functional changes in presynaptic DA neurons in ARHGAP10$^{NHEJ/S490P}$ mice are
395 minimal and may not play a significant role in the higher sensitivity to METH in
396 ARHGAP10$^{NHEJ/S490P}$ mice.
397 Neurons in the ST and NAc of ARHGAP10$^{NHEJ/S490P}$ mice exhibit more complex
398 morphology (**Fig. 3**) and higher spine density including mushroom-type mature spines (**Fig. 4**)
399 compared with those in WT mice. Accordingly, these postsynaptic changes in the ST and NAc
400 may be related to the higher sensitivity and enhanced response to METH in
401 ARHGAP10$^{NHEJ/S490P}$ mice. To test our hypothesis, the number of c-Fos-positive cells was
402 compared in the dorsomedial ST, dorsolateral ST, NAc core, and NAc shell between
403 ARHGAP10$^{NHEJ/S490P}$ and WT mice following METH (0.3 mg/kg) treatment. Quantitative
404 analyses revealed that METH (0.3 mg/kg) significantly increased the number of c-Fos-positive
405 cells in the dorsomedial ST (genotype, $F_{(1, 8)} = 3.19$, $p = 0.112$, treatment, $F_{(1, 8)} = 37.4$, $p < 0.01$,
406 genotype×treatment interaction, $F_{(1, 8)} = 20.9$, $p < 0.01$, two-way ANOVA, **Fig. 6a**) and NAc
407 core (genotype, $F_{(1, 8)} = 6.78$, $p < 0.05$, treatment, $F_{(1, 8)} = 4.41$, $p = 0.069$, genotype×treatment
408 interaction, $F_{(1, 8)} = 8.16$, $p < 0.05$, two-way ANOVA, **Fig. 6c**) in ARHGAP10$^{NHEJ/S490P}$ mice but
409 not WT mice. No significant differences were observed in the dorsolateral ST (genotype, $F_{(1, 8)} =$
410 1.17, $p = 0.311$, treatment, $F_{(1, 8)} = 0.23$, $p = 0.644$, genotype×treatment interaction, $F_{(1, 8)} = 0.13$,
411 $p = 0.728$, two-way ANOVA, **Fig. 6b**) and NAc shell (genotype, $F_{(1, 8)} = 0.89$, $p = 0.374$,
412 treatment, $F_{(1, 8)} = 1.33$, $p = 0.283$, genotype×treatment interaction, $F_{(1, 8)} = 3.55$, $p = 0.096$, two-
413 way ANOVA, **Fig. 6d**) between METH-treated WT and ARHGAP10$^{NHEJ/S490P}$ mice. Taken

414 together, the higher sensitivity and enhanced response to METH in ARHGAP10$^{NHEJ/S490P}$ mice
415 may be associated with the morphological abnormality of neurons in the dorsomedial ST and
416 NAc core.
417
418 **Discussion**
419 In the present study, we demonstrated that *Arhgap10* gene expression increases postnatally in an
420 age-dependent manner in the mouse brain, in which the highest expression was observed in the
421 ST and NAc in adulthood. It is well known that 95% of neurons within the ST and NAc are
422 medium spiny neurons (MSNs), which are a special type of GABAergic inhibitory cell [51, 52].
423 Thus, it is possible that the *Arhgap10* gene may be expressed in MSNs of the ST and NAc in
424 adulthood.
425 ARHGAP10 participates in the regulation of RhoA and Cdc42 activity [20]. Deletions
426 of RhoA GAP genes, such as Oligophrenin1 and p190RhoGAP, led to an increase in RhoA
427 activity, whereas deletion of the SNX26 gene, which belongs to Cdc42 GAP family, resulted in
428 activation of Cdc42 signal [53-55]. *In vitro* experiments have already demonstrated that the
429 *Arhgap10* S490P mutation increases RhoA activity due to a resultant decrease in the interaction
430 of ARHGAP10 with GTP-RhoA [13]. In this study, we observed that not only phospho-MYPT1
431 levels but also phospho-PAK1/2 levels were upregulated in the ST and NAc of
432 ARHGAP10$^{NHEJ/S490P}$ mice. These findings suggested that RhoA and Cdc42 signaling was
433 promoted in the ST and NAc of ARHGAP10$^{NHEJ/S490P}$ mice, namely the *Arhgap10* gene
434 mutations may be accelerating RhoA and Cdc42 signals in MSNs.
435 Postmortem studies revealed that the spine density of cortical parts is decreased in SCZ
436 patients [56, 57], whereas dendritic synaptic density in the ST is increased [58]. Similarly, a

437 significant decrease in spine density in the medial prefrontal cortex of ARHGAP10$^{NHEJ/S490P}$
438 mice was reported in our previous study [13], whereas a significant increase in spine density as
439 well as neuronal complexity in the ST and NAc was demonstrated in the present study. Rho
440 signaling controls neuronal branching pattern and dendritic spine density [59-63]. Constitutive
441 active RhoA decreases spine density, whereas activation of Cdc42 increases spine density [55,
442 59, 61, 62]. These findings suggested that the contribution of Rho signals regulated by
443 ARHGAP10 is different in the medial prefrontal cortex and ST. Further studies are required to
444 conclude a causal association between the *Arhgap10* mutation and neuronal morphology in
445 MSNs.

446 Changes in dendritic spine shape have been correlated with behavioral alterations, such
447 as learning and memory, and may provide a structural basis for plasticity in the brain [64].
448 Structural changes in spines can occur within seconds and are coupled to changes in synaptic
449 activity [65]. Previous reports indicated RhoA and Cdc42 activation in single dendritic spines
450 undergoing structural plasticity associated with LTP [66, 67]. The dendritic spine shape is
451 classified and synaptic ability is different among them [41, 44-46]. Mushroom-type spines
452 represents a more mature population than other types of spines, and their large head/neck ratio is
453 thought to contribute to their function as stable excitatory synapses [65]. Of note, repetitive
454 AMPH or METH treatment induces behavioral sensitization in mice [68, 69], which is
455 accompanied by an increase in mushroom-type spine density in MSNs [70, 71]. In the present
456 study, we found an increase in mushroom-type spine density in the ST and NAc neurons of
457 ARHGAP10$^{NHEJ/S490P}$ mice that have a higher sensitivity to METH. These results suggested that
458 morphological abnormalities in the ST and NAc of ARHGAP10$^{NHEJ/S490P}$ mice may be related to
459 their hypersensitivity to METH. MSNs in the ST and NAc receive dopaminergic input from the

SN/VTA, as well as excitatory glutamatergic input from the cortex/thalamus [72]. In the present study, an *in vivo* microdialysis study showed that basal and METH-induced DA release in the NAc of ARHGAP10$^{NHEJ/S490P}$ mice were comparable to those in WT mice, indicating that the function of the mesostriatal DA pathway is normal in ARHGAP10$^{NHEJ/S490P}$ mice.

The touchscreen-based VD task can be used to assess aspects of associative learning and perceptual ability in rodent [28], and visual perception and recognition is impaired in SCZ patients [73]. Brigman et al. (2013) reported that the principal brain regions are activated during choice behavior. An excitotoxic lesion as well as *in vivo* neuronal recording suggested that normal performance in the VD task depends on the intact function of the cortico–striato–thalamic circuitry. The neuronal circuit for this type of learning behaviors is preserved in humans, non-human primates, and rodents [74]. ARHGAP10$^{NHEJ/S490P}$ mice showed normal performance in the VD and reversal learning task, indicating that learning ability may be normal in ARHGAP10$^{NHEJ/S490P}$ mice. Nevertheless, a low dose of METH impaired VD performance in ARHGAP10$^{NHEJ/S490P}$ mice but not WT mice, although there was no difference in METH-induced DA release between the two groups. Furthermore, ARHGAP10$^{NHEJ/S490P}$ mice have an abnormality in the morphology of striatal MSNs with a higher density of mushroom-type mature spines compared with WT mice. Thus, the MSNs in the ST/NAc of ARHGAP10$^{NHEJ/S490P}$ mice may exhibit abnormal responses upon DA receptor stimulation after METH administration. This hypothesis was consistent with clinical findings that SCZ patients are sensitive to METH [75].

c-Fos expression analysis suggested that the dorsomedial ST and NAc core neurons of ARHGAP10$^{NHEJ/S490P}$ mice are hypersensitive to METH. A previous study reported that dopamine D2 receptors (D2Rs) have a much higher affinity for DA than dopamine D1 receptors (D1Rs) [76]. Therefore, D2Rs are more activated than D1Rs in basal DA levels and are more

483 sensitive to DA pauses, whereas D1Rs are more sensitive to DA bursts, in conditions with higher
484 DA release, which predominantly increases the activation of stimulatory D1Rs. Consistent with
485 this, D1R-MSNs are less excitable than D2R-MSNs and the activity of D2R-MSNs may
486 predominate in basal conditions [77]. Conversely, D1R-MSNs become more excitable when DA
487 levels are substantially increased by repetitive psychostimulant administration, and result in
488 enhanced responses to excitatory inputs. Following an increase in excitability, D1R-MSNs
489 promote accumbal processing of excitatory glutamatergic input [78, 79]. Therefore, we
490 hypothesized that METH-induced impairment of VD may be due to D1R-MSNs abnormality in
491 ARHGAP10$^{NHEJ/S490P}$ mice. Further studies are needed to confirm this working hypothesis.
492 In conclusion, our results suggested that *Arhgap10* gene mutations have a
493 pathophysiologic and pathogenic role, involving structural and functional changes in ST and
494 NAc MSNs, in SCZ. Targeting the regulation of Rho GTPase and the downstream signaling may
495 provide new therapeutic approaches for the treatment of SCZ patients with *Arhgap10* gene
496 mutations.
497
498 **Declarations**
499 **List of abbreviations**
500 aCSF: artificial cerebrospinal fluid; AMPH: amphetamine; ANOVA: analysis of variance;
501 ARHGAP10: rho GTPase activating protein 10; CNVs: copy-number variations; D1Rs:
502 dopamine D1 receptors; D2Rs: dopamine D2 receptors; DA: dopamine; Fc: frontal cortex;
503 GAPs: rho GTPase activating proteins; Hip: hippocampus; HRP: horseradish peroxidase; ISH: *in*
504 *situ* hybridization; PAKs: p21-activated kinases; PB: phosphate buffer; PBS: phosphate-buffered
505 saline; PFA: paraformaldehyde; Rn: raphe nuclei; ROCK: Rho-kinase; RT: room temperature;

RT-qPCR: reverse transcription quantitative real-time polymerase chain reaction; SCZ: schizophrenia; SN/VTA: substantia nigra/ventral tegmental area; ST: striatum; TBS: tris-buffered saline; METH: methamphetamine; MLC: myosin light chain; MSNs: medium spiny neurons; MYPT1: myosin phosphatase-targeting subunit 1; NAc: nucleus accumbens; NBF: neutral buffered formalin; NHEJ: non-homologous end-joining; VD: visual discrimination; WT: wild-type

Ethics approval and consent to participate

All of the animal experiments were approved and performed in accordance with the guidelines of the Animal Care and Use Committee of Nagoya University Graduate School of Medicine (approval number: 31361).

Consent for publication

Not applicable.

Availability of data and materials

All data generated or analyzed during this study are included in this published article. Additional inquiries can be directed to the corresponding author.

Competing interests

The authors declare that they have no competing interests.

Funding

This study was supported by AMED under grant Nos. JP20ak0101113, JP20ak0101126, JP20dm0107087, JP20dm0107160, JP20dm0207075, JP20dk0307075, JP20dk0307081, JP20ek0109411, and JP20km0405216; Japan Society for the Promotion of Science (JSPS) KAKENHI Grant Numbers 17H02220, 17H04031, 17H04252, 20H03428, 20K07082; and the Uehara Memorial Foundation.

Authors' contributions

K.H.:molecular analysis, B.W. :animal analysis, T.N.:study design were equally contributed to this study. K.H. performed molecular biology experiments; B.W. performed animal studies; K.H., B.W., T.N., N.I., M.S., A.S., H.M., D.M., I.K., T.N., N.O., and K.Y. designed the study and wrote the manuscript.

Acknowledgements

We thank the staff of the Division of Experimental Animals, Nagoya University Graduate School of Medicine for their technical support and the Division for Medical Research Engineering, Nagoya University Graduate School of Medicine, for usage of the fluorescence microscopy system (BZ9000) and image analysis software.

Figure Captions

Figure 1. Spatiotemporal expression of *Arhgap10* in the mouse brain

(a) Temporal changes in *Arhgap10* mRNA levels in the hippocampus (Hip) and frontal cortex (Fc) of C57BL/6J mice (n = 3 mice in each group). (b) Expression of *Arhgap10* mRNA levels in the Hip, Fc, striatum (ST), nucleus accumbens (NAc), substantia nigra/ventral tegmental area

(SN/VTA), and raphe nuclei (Rn) of C57BL/6J mice at P56 (n = 3 mice). (c) Representative images showing *Arhgap10* mRNA expression at P56 by ISH. Scale bar indicates 1 mm. (d) Higher magnification of *Arhgap10* mRNA signals in the Fc, Hip, ST, and SN/VTA of the mouse brain. Scale bar indicates 50 μm. **p < 0.01.

Figure 2. Activation of MYPT1 and PAKs in the ST and NAc of ARHGAP10$^{NHEJ/S490P}$ mice

(a, d) Representative endogenous protein levels of phosphorylated (upper) and total band (lower) of MYPT1 (a) and PAK1/2 (d) in the ST and NAc. (b, c, e, f) Quantification of phosphorylated band intensity in the ST and NAc was normalized to total (b, e) MYPT1 and (c, f) PAK1/2 band, respectively. * p < 0.05, ** p < 0.01. All data are expressed as means ± SEM (MYPT1; n = 8 mice, PAK1/2; n = 8 mice in each genotype).

Figure 3. Abnormal neuronal morphology in the ST and NAc of ARHGAP10$^{NHEJ/S490P}$ mice

(a, f) Representative images of Golgi-stained single neurons in the ST (a) and NAc (f). Scale bar: upper panel 300 μm and lower panel 10 μm. (b–e, g–j) quantitative analyses of (b, g) intersection, (c, h) length, (d, i) nodes, (e, j) ending in the (b–e) ST and (g–j) NAc. *p < 0.05, ** p < 0.01. All data are expressed as means ± SEM (n = 8–15 neurons from 4–5 mice in each genotype).

Figure 4. Changes in spine density and morphology in the ST and NAc of ARHGAP10$^{NHEJ/S490P}$ mice

(a) Representative images of the ST and NAc dendric spines (Scale bar indicates 10 μm). (b) Spine densities of the ST and NAc neurons. (c) Representative images of a dendritic segment illustrating different spine subtypes in NAc. (d–k) Quantification of dendritic spine: (d, h)

mushroom, (e, i) thin, (f, j) stubby, and (g, k) brunched types in the (d-g) ST and (h-k) NAc neurons, respectively. ** $p < 0.01$. All data are expressed as means ± SEM (n = 16 neurons from 4 mice in each genotype).

Figure 5. Impairment of VD in ARHGAP10$^{NHEJ/S490P}$ mice induced by METH

(a) Mice were administered METH (0.3 or 1.0 mg/kg. i.p.) 30 min before the VD task. (b) Total number of trials to reach the learning criterion in VD task. (c) Percentage of the correct response. (d) Percentage of trials completed. (e) Time to correct response. (f) Time to reward retrieval. *$p < 0.05$, ** $p < 0.01$. All data are expressed as means ± SEM (WT mice n = 6, ARHGAP10$^{NHEJ/S490P}$ mice n = 7).

Figure 6. METH-induced changes in neuronal activity of the dorsal ST and NAc in ARHGAP10$^{NHEJ/S490P}$ mice

(a-d) Representative images and the number of c-Fos-positive cells in the (a) dorsomedial ST, (b) dorsolateral ST, (c) NAc core and (d) NAc shell. Scale bar indicates 100 μm. *$p < 0.05$, ** $p < 0.01$. All data are expressed as means ± SEM (n = 9 slices from 3 mice in each group).

Additional file 1: Figure S1. Performance of ARHGAP10$^{NHEJ/S490P}$ mice in the VD reversal learning task.

(a) Percentage of correct responses in reversal learning (genotype, $F_{(1, 7)} = 0.35$, $p = 0.57$, day, $F_{(8, 56)} = 22.5$, $p < 0.01$, genotype×day interaction, $F_{(8, 56)} = 0.31$, $p = 0.96$). (b) Total trials to reversal learning criteria ($p = 0.62$, Mann–Whitney U-test). All data are expressed as means ± SEM (WT mice n = 4, ARHGAP10$^{NHEJ/S490P}$ mice n = 5).

Additional file 2: Figure S2. METH-induced DA release in the NAc of ARHGAP10$^{NHEJ/S490P}$ mice.

(a) Basal extracellular levels of DA (p = 0.15, Mann–Whitney U-test) and (b) METH-induced (1 mg/kg, i.p.) DA release (genotype, $F_{(1, 10)}$ = 0.9, p = 0.36, time, $F_{(43, 430)}$ = 22.8, p < 0.01, genotype×time interaction, $F_{(43, 430)}$ = 0.5, p = 1.0) in the NA of ARHGAP10$^{NHEJ/S490P}$ mice were determined using a microdialysis method. Each fraction was collected for 5 min. All data are expressed as means ± SEM (n = 6 mice in each genotype).

References

1. Kendler KS, Diehl SR. The genetics of schizophrenia: a current, genetic-epidemiologic perspective. Schizophr Bull. 1993;19:261-85.
2. Caspi A, Moffitt TE. Gene-environment interactions in psychiatry: joining forces with neuroscience. Nat Rev Neurosci. 2006;7:583-90.
3. Jaffee SR, Price TS. Gene-environment correlations: a review of the evidence and implications for prevention of mental illness. Mol Psychiatry. 2007;12:432-42.
4. Patterson PH. Neuroscience. Maternal effects on schizophrenia risk. Science. 2007;318:576-7.
5. Xu MQ, Sun WS, Liu BX, Feng GY, Yu L, Yang L, et al. Prenatal malnutrition and adult schizophrenia: further evidence from the 1959-1961 Chinese famine. Schizophr Bull. 2009;35:568-76.

6. Zammit S, Allebeck P, Andreasson S, Lundberg I, Lewis G. Self reported cannabis use as a risk factor for schizophrenia in Swedish conscripts of 1969: historical cohort study. Bmj. 2002;325:1199.
7. Doherty JL, Owen MJ. Genomic insights into the overlap between psychiatric disorders: implications for research and clinical practice. Genome Med. 2014;6:29.
8. Kushima I, Aleksic B, Nakatochi M, Shimamura T, Okada T, Uno Y, et al. Comparative analyses of copy-number variation in autism spectrum disorder and schizophrenia reveal etiological overlap and biological insights. Cell Rep. 2018;24:2838-56.
9. Kushima I, Aleksic B, Nakatochi M, Shimamura T, Shiino T, Yoshimi A, et al. High-resolution copy number variation analysis of schizophrenia in Japan. Mol Psychiatry. 2017;22:430-40.
10. Marshall CR, Howrigan DP, Merico D, Thiruvahindrapuram B, Wu W, Greer DS, et al. Contribution of copy number variants to schizophrenia from a genome-wide study of 41,321 subjects. Nat Genet. 2017;49:27-35.
11. Moreno-De-Luca A, Myers SM, Challman TD, Moreno-De-Luca D, Evans DW, Ledbetter DH. Developmental brain dysfunction: revival and expansion of old concepts based on new genetic evidence. Lancet Neurol. 2013;12:406-14.
12. Saito R, Koebis M, Nagai T, Shimizu K, Liao J, Wulaer B, et al. Comprehensive analysis of a novel mouse model of the 22q11.2 deletion syndrome: a model with the most common 3.0-Mb deletion at the human 22q11.2 locus. Transl Psychiatry. 2020;10:35.
13. Sekiguchi M, Sobue A, Kushima I, Wang C, Arioka Y, Kato H, et al. ARHGAP10, which encodes Rho GTPase-activating protein 10, is a novel gene for schizophrenia risk. Transl Psychiatry. 2020;10:247.

14. Basseres DS, Tizzei EV, Duarte AA, Costa FF, Saad ST. ARHGAP10, a novel human gene coding for a potentially cytoskeletal Rho-GTPase activating protein. Biochem Biophys Res Commun. 2002;294:579-85.
15. Shibata H, Oishi K, Yamagiwa A, Matsumoto M, Mukai H, Ono Y. PKNβ interacts with the SH3 domains of Graf and a novel Graf related protein, Graf2, which are GTPase activating proteins for Rho family. J Biochem. 2001;130:23-31.
16. Vorstman JAS, Olde Loohuis LM, Kahn RS, Ophoff RA. Double hits in schizophrenia. Hum Mol Genet. 2018;27:2755-61.
17. Black JE, Kodish IM, Grossman AW, Klintsova AY, Orlovskaya D, Vostrikov V, et al. Pathology of layer V pyramidal neurons in the prefrontal cortex of patients with schizophrenia. Am J Psychiatry. 2004;161:742-4.
18. Konopaske GT, Lange N, Coyle JT, Benes FM. Prefrontal cortical dendritic spine pathology in schizophrenia and bipolar disorder. JAMA Psychiatry. 2014;71:1323-31.
19. Moyer CE, Shelton MA, Sweet RA. Dendritic spine alterations in schizophrenia. Neurosci Lett. 2015;601:46-53.
20. Ren XR, Du QS, Huang YZ, Ao SZ, Mei L, Xiong WC. Regulation of CDC42 GTPase by proline-rich tyrosine kinase 2 interacting with PSGAP, a novel pleckstrin homology and Src homology 3 domain containing rhoGAP protein. J Cell Biol. 2001;152:971-84.
21. Curran C, Byrappa N, McBride A. Stimulant psychosis: systematic review. Br J Psychiatry. 2004;185:196-204.
22. Lieberman JA, Kane JM, Alvir J. Provocative tests with psychostimulant drugs in schizophrenia. Psychopharmacology (Berl). 1987;91:415-33.

23. Sobue A, Ito N, Nagai T, Shan W, Hada K, Nakajima A, et al. Astroglial major histocompatibility complex class I following immune activation leads to behavioral and neuropathological changes. Glia. 2018;66:1034-52.

24. Nakai T, Nagai T, Tanaka M, Itoh N, Asai N, Enomoto A, et al. Girdin phosphorylation is crucial for synaptic plasticity and memory: a potential role in the interaction of BDNF/TrkB/Akt signaling with NMDA receptor. J Neurosci. 2014;34:14995-5008.

25. Nagai T, Yamada K, Yoshimura M, Ishikawa K, Miyamoto Y, Hashimoto K, et al. The tissue plasminogen activator-plasmin system participates in the rewarding effect of morphine by regulating dopamine release. Proc Natl Acad Sci U S A. 2004;101:3650-5.

26. Wulaer B, Nagai T, Sobue A, Itoh N, Kuroda K, Kaibuchi K, et al. Repetitive and compulsive-like behaviors lead to cognitive dysfunction in Disc1$^{(\Delta 2\text{-}3/\Delta 2\text{-}3)}$ mice. Genes Brain Behav. 2018;17:e12478.

27. Dietz DM, Sun H, Lobo MK, Cahill ME, Chadwick B, Gao V, et al. Rac1 is essential in cocaine-induced structural plasticity of nucleus accumbens neurons. Nat Neurosci. 2012;15:891-6.

28. Horner AE, Heath CJ, Hvoslef-Eide M, Kent BA, Kim CH, Nilsson SR, et al. The touchscreen operant platform for testing learning and memory in rats and mice. Nat Protoc. 2013;8:1961-84.

29. Kim J, Shim S, Choi SC, Han JK. A putative Xenopus Rho-GTPase activating protein (XrGAP) gene is expressed in the notochord and brain during the early embryogenesis. Gene Expr Patterns. 2003;3:219-23.

30. Carter CS, Perlstein W, Ganguli R, Brar J, Mintun M, Cohen JD. Functional hypofrontality and working memory dysfunction in schizophrenia. Am J Psychiatry. 1998;155:1285-7.

31. Heckers S, Konradi C. Hippocampal neurons in schizophrenia. J Neural Transm (Vienna). 2002;109:891-905.

32. Reynolds GP, Beasley CL. GABAergic neuronal subtypes in the human frontal cortex--development and deficits in schizophrenia. J Chem Neuroanat. 2001;22:95-100.

33. Weinberger DR. Cell biology of the hippocampal formation in schizophrenia. Biol Psychiatry. 1999;45:395-402.

34. Weinberger DR, Egan MF, Bertolino A, Callicott JH, Mattay VS, Lipska BK, et al. Prefrontal neurons and the genetics of schizophrenia. Biol Psychiatry. 2001;50:825-44.

35. Kimura K, Ito M, Amano M, Chihara K, Fukata Y, Nakafuku M, et al. Regulation of myosin phosphatase by Rho and Rho-associated kinase (Rho-kinase). Science. 1996;273:245-8.

36. Chong C, Tan L, Lim L, Manser E. The mechanism of PAK activation. Autophosphorylation events in both regulatory and kinase domains control activity. J Biol Chem. 2001;276:17347-53.

37. Govek EE, Newey SE, Van Aelst L. The role of the Rho GTPases in neuronal development. Genes Dev. 2005;19:1-49.

38. Amano M, Nakayama M, Kaibuchi K. Rho-kinase/ROCK: A key regulator of the cytoskeleton and cell polarity. Cytoskeleton (Hoboken). 2010;67:545-54.

39. Calabrese B, Wilson MS, Halpain S. Development and regulation of dendritic spine synapses. Physiology (Bethesda). 2006;21:38-47.

40. Negishi M, Katoh H. Rho family GTPases and dendrite plasticity. Neuroscientist. 2005;11:187-91.

41. Bourne JN, Harris KM. Balancing structure and function at hippocampal dendritic spines. Annu Rev Neurosci. 2008;31:47-67.

42. Tada T, Sheng M. Molecular mechanisms of dendritic spine morphogenesis. Curr Opin Neurobiol. 2006;16:95-101.

43. Risher WC, Ustunkaya T, Singh Alvarado J, Eroglu C. Rapid Golgi analysis method for efficient and unbiased classification of dendritic spines. PLoS One. 2014;9:e107591.

44. Harris KM, Jensen FE, Tsao B. Three-dimensional structure of dendritic spines and synapses in rat hippocampus (CA1) at postnatal day 15 and adult ages: implications for the maturation of synaptic physiology and long-term potentiation. J Neurosci. 1992;12:2685-705.

45. Lohmann C, Finski A, Bonhoeffer T. Local calcium transients regulate the spontaneous motility of dendritic filopodia. Nat Neurosci. 2005;8:305-12.

46. Zito K, Scheuss V, Knott G, Hill T, Svoboda K. Rapid functional maturation of nascent dendritic spines. Neuron. 2009;61:247-58.

47. Brigman JL, Daut RA, Wright T, Gunduz-Cinar O, Graybeal C, Davis MI, et al. GluN2B in corticostriatal circuits governs choice learning and choice shifting. Nat Neurosci. 2013;16:1101-10.

48. Talpos JC, Fletcher AC, Circelli C, Tricklebank MD, Dix SL. The pharmacological sensitivity of a touchscreen-based visual discrimination task in the rat using simple and perceptually challenging stimuli. Psychopharmacology (Berl). 2012;221:437-49.

49. Carboni E, Spielewoy C, Vacca C, Nosten-Bertrand M, Giros B, Di Chiara G. Cocaine and amphetamine increase extracellular dopamine in the nucleus accumbens of mice lacking the dopamine transporter gene. J Neurosci. 2001;21:Rc141: 1-4.

50. Wheeler DS, Underhill SM, Stolz DB, Murdoch GH, Thiels E, Romero G, et al. Amphetamine activates Rho GTPase signaling to mediate dopamine transporter internalization and acute behavioral effects of amphetamine. Proc Natl Acad Sci U S A. 2015;112:E7138-47.

51. Graveland GA, DiFiglia M. The frequency and distribution of medium-sized neurons with indented nuclei in the primate and rodent neostriatum. Brain Res. 1985;327:307-11.

52. Kreitzer AC. Physiology and pharmacology of striatal neurons. Annu Rev Neurosci. 2009;32:127-47.

53. Arthur WT, Burridge K. RhoA inactivation by p190RhoGAP regulates cell spreading and migration by promoting membrane protrusion and polarity. Mol Biol Cell. 2001;12:2711-20.

54. Khelfaoui M, Gambino F, Houbaert X, Ragazzon B, Muller C, Carta M, et al. Lack of the presynaptic RhoGAP protein oligophrenin1 leads to cognitive disabilities through dysregulation of the cAMP/PKA signalling pathway. Philos Trans R Soc Lond B Biol Sci. 2014;369:20130160.

55. Kim Y, Ha CM, Chang S. SNX26, a GTPase-activating protein for Cdc42, interacts with PSD-95 protein and is involved in activity-dependent dendritic spine formation in mature neurons. J Biol Chem. 2013;288:29453-66.

56. Garey LJ, Ong WY, Patel TS, Kanani M, Davis A, Mortimer AM, et al. Reduced dendritic spine density on cerebral cortical pyramidal neurons in schizophrenia. J Neurol Neurosurg Psychiatry. 1998;65:446-53.

57. Glantz LA, Lewis DA. Decreased dendritic spine density on prefrontal cortical pyramidal neurons in schizophrenia. Arch Gen Psychiatry. 2000;57:65-73.

58. Roberts RC, Roche JK, Conley RR. Synaptic differences in the postmortem striatum of subjects with schizophrenia: a stereological ultrastructural analysis. Synapse. 2005;56:185-97.

59. Fox ME, Chandra R, Menken MS, Larkin EJ, Nam H, Engeln M, et al. Dendritic remodeling of D1 neurons by RhoA/Rho-kinase mediates depression-like behavior. Mol Psychiatry. 2018.

60. Irie F, Yamaguchi Y. EphB receptors regulate dendritic spine development via intersectin, Cdc42 and N-WASP. Nat Neurosci. 2002;5:1117-8.

61. Lesiak A, Pelz C, Ando H, Zhu M, Davare M, Lambert TJ, et al. A genome-wide screen of CREB occupancy identifies the RhoA inhibitors Par6C and Rnd3 as regulators of BDNF-induced synaptogenesis. PLoS One. 2013;8:e64658.

62. Sarner S, Kozma R, Ahmed S, Lim L. Phosphatidylinositol 3-kinase, Cdc42, and Rac1 act downstream of Ras in integrin-dependent neurite outgrowth in N1E-115 neuroblastoma cells. Mol Cell Biol. 2000;20:158-72.

63. Vadodaria KC, Brakebusch C, Suter U, Jessberger S. Stage-specific functions of the small Rho GTPases Cdc42 and Rac1 for adult hippocampal neurogenesis. J Neurosci. 2013;33:1179-89.

64. Mahmmoud RR, Sase S, Aher YD, Sase A, Groger M, Mokhtar M, et al. Spatial and working memory is linked to spine density and mushroom spines. PLoS One. 2015;10:e0139739.
65. Matsuzaki M, Ellis-Davies GC, Nemoto T, Miyashita Y, Iino M, Kasai H. Dendritic spine geometry is critical for AMPA receptor expression in hippocampal CA1 pyramidal neurons. Nat Neurosci. 2001;4:1086-92.
66. Hedrick NG, Harward SC, Hall CE, Murakoshi H, McNamara JO, Yasuda R. Rho GTPase complementation underlies BDNF-dependent homo- and heterosynaptic plasticity. Nature. 2016;538:104-8.
67. Murakoshi H, Wang H, Yasuda R. Local, persistent activation of Rho GTPases during plasticity of single dendritic spines. Nature. 2011;472:100-4.
68. Kamei H, Nagai T, Nakano H, Togan Y, Takayanagi M, Takahashi K, et al. Repeated methamphetamine treatment impairs recognition memory through a failure of novelty-induced ERK1/2 activation in the prefrontal cortex of mice. Biol Psychiatry. 2006;59:75-84.
69. Nagai T, Noda Y, Ishikawa K, Miyamoto Y, Yoshimura M, Ito M, et al. The role of tissue plasminogen activator in methamphetamine-related reward and sensitization. J Neurochem. 2005;92:660-7.
70. Ferreras S, Fernandez G, Danelon V, Pisano MV, Masseroni L, Chapleau CA, et al. Cdk5 is essential for amphetamine to increase dendritic spine density in hippocampal pyramidal neurons. Front Cell Neurosci. 2017;11:372.
71. Tu G, Ying L, Ye L, Zhao J, Liu N, Li J, et al. Dopamine D1 and D2 receptors differentially regulate Rac1 and Cdc42 signaling in the nucleus accumbens to modulate

behavioral and structural plasticity after repeated methamphetamine treatment. Biol Psychiatry. 2019;86:820-35.

72. Gardoni F, Bellone C. Modulation of the glutamatergic transmission by dopamine: a focus on Parkinson, Huntington and Addiction diseases. Front Cell Neurosci. 2015;9:25.

73. O'Donnell BF, Swearer JM, Smith LT, Nestor PG, Shenton ME, McCarley RW. Selective deficits in visual perception and recognition in schizophrenia. Am J Psychiatry. 1996;153:687-92.

74. Haber SN. The place of dopamine in the cortico-basal ganglia circuit. Neuroscience. 2014;282:248-57.

75. Angrist B, Rotrosen J, Gershon S. Differential effects of amphetamine and neuroleptics on negative vs. positive symptoms in schizophrenia. Psychopharmacology (Berl). 1980;72:17-9.

76. Seamans JK, Yang CR. The principal features and mechanisms of dopamine modulation in the prefrontal cortex. Prog Neurobiol. 2004;74:1-58.

77. Richfield EK, Penney JB, Young AB. Anatomical and affinity state comparisons between dopamine D1 and D2 receptors in the rat central nervous system. Neuroscience. 1989;30:767-77.

78. Nagai T, Nakamuta S, Kuroda K, Nakauchi S, Nishioka T, Takano T, et al. Phosphoproteomics of the dopamine pathway enables discovery of Rap1 activation as a reward signal in vivo. Neuron. 2016;89:550-65.

79. Surmeier DJ, Ding J, Day M, Wang Z, Shen W. D1 and D2 dopamine-receptor modulation of striatal glutamatergic signaling in striatal medium spiny neurons. Trends Neurosci. 2007;30:228-35.

Figures

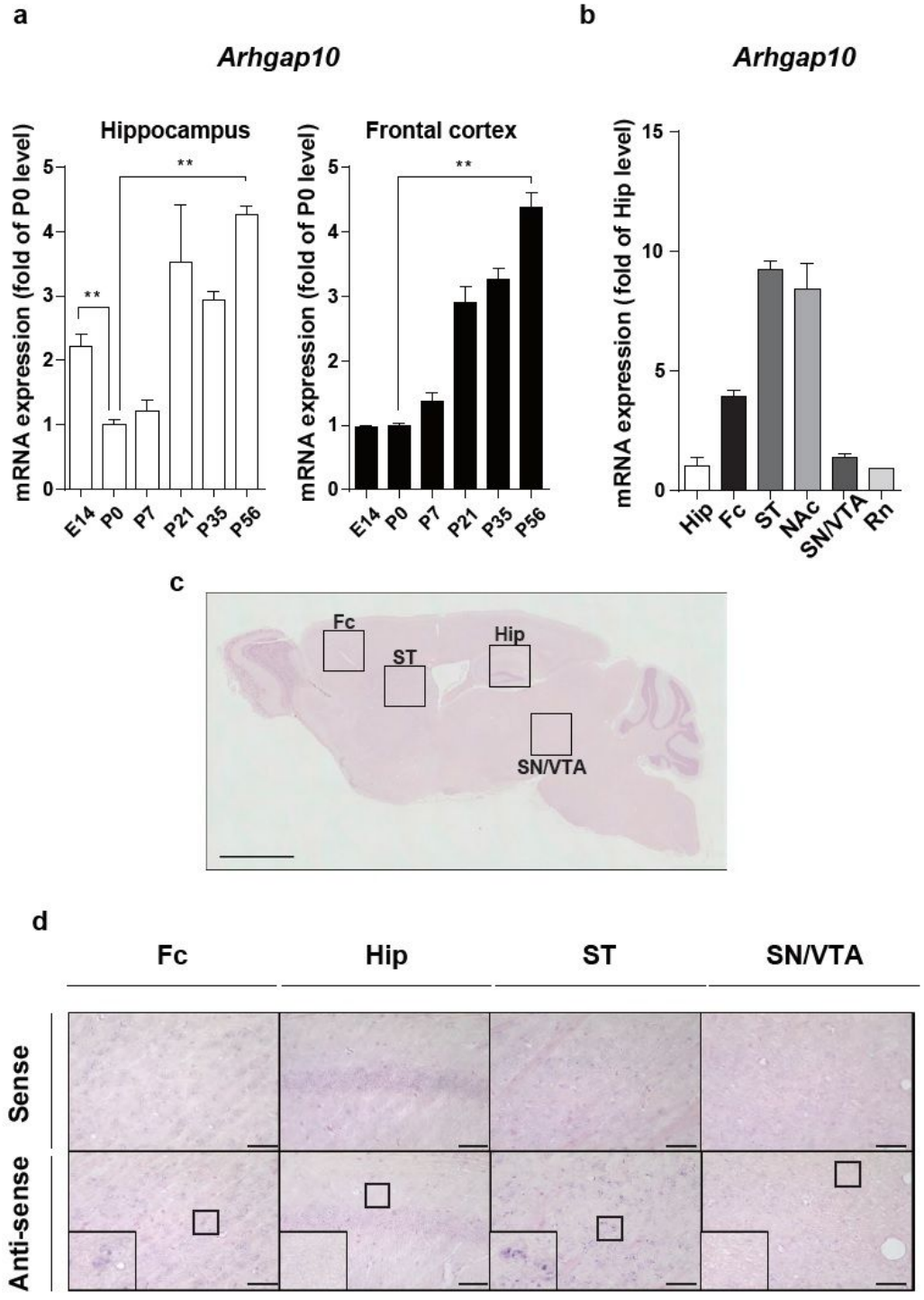

Figure 1

Spatiotemporal expression of Arhgap10 in the mouse brain (a) Temporal changes in Arhgap10 mRNA levels in the hippocampus (Hip) and frontal cortex (Fc) of C57BL/6J mice (n = 3 mice in each group). (b) Expression of Arhgap10 mRNA levels in the Hip, Fc, striatum (ST), nucleus accumbens (NAc), substantia

nigra/ventral tegmental area (SN/VTA), and raphe nuclei (Rn) of C57BL/6J mice at P56 (n = 3 mice). (c) Representative images showing Arhgap10 mRNA expression at P56 by ISH. Scale bar indicates 1 mm. (d) Higher magnification of Arhgap10 mRNA signals in the Fc, Hip, ST, and SN/VTA of the mouse brain. Scale bar indicates 50 um. **p < 0.01.

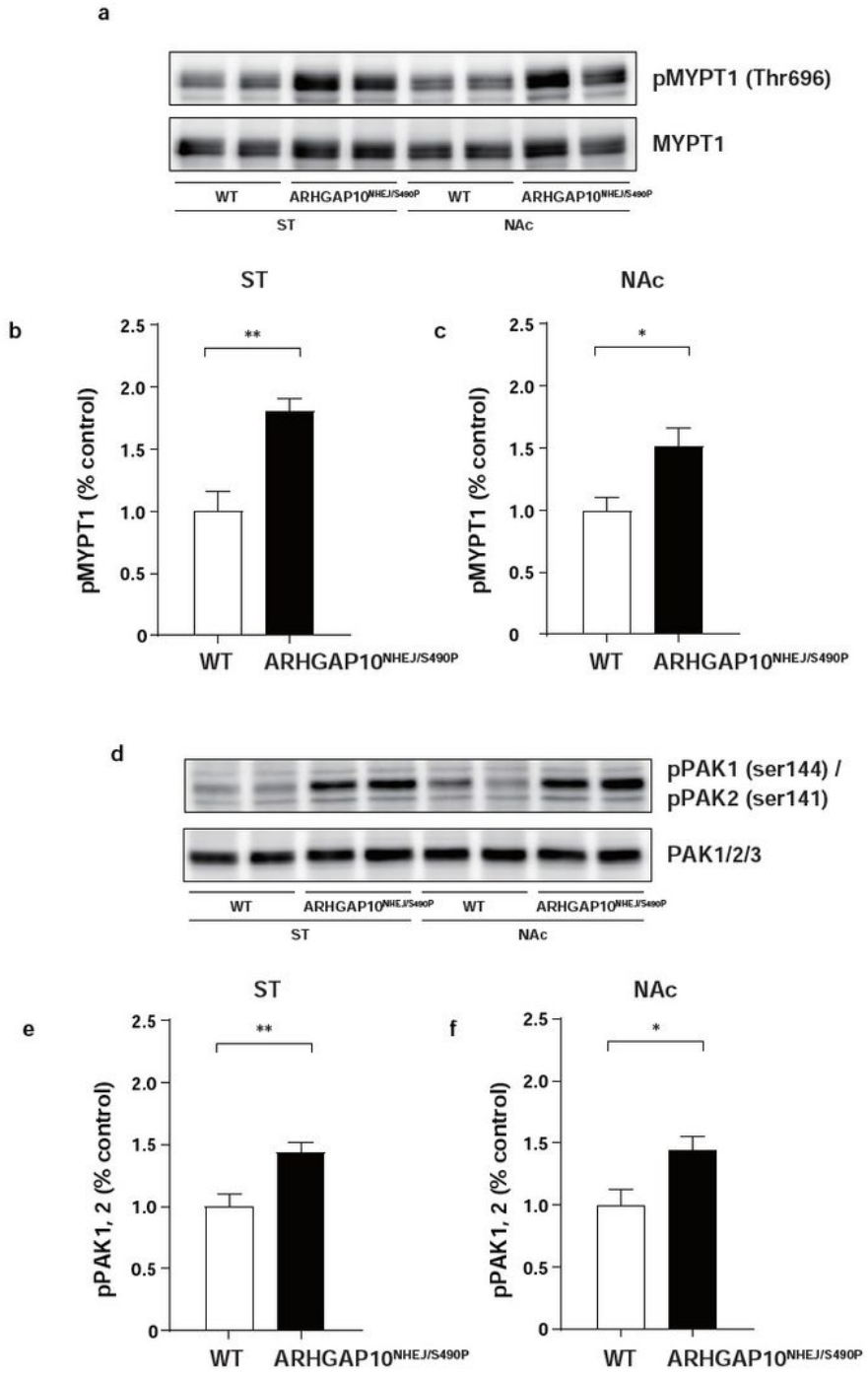

Figure 2

Activation of MYPT1 and PAKs in the ST and NAc of ARHGAP10NHEJ/S490P mice (a, d) Representative endogenous protein levels of phosphorylated (upper) and total band (lower) of MYPT1 (a) and PAK1/2 (d) in the ST and NAc. (b, c, e, f) Quantification of phosphorylated band intensity in the ST and NAc was normalized to total (b, e) MYPT1 and (c, f) PAK1/2 band, respectively. * $p < 0.05$, ** $p < 0.01$. All data are expressed as means ± SEM (MYPT1; n = 8 mice, PAK1/2; n = 8 mice in each genotype).

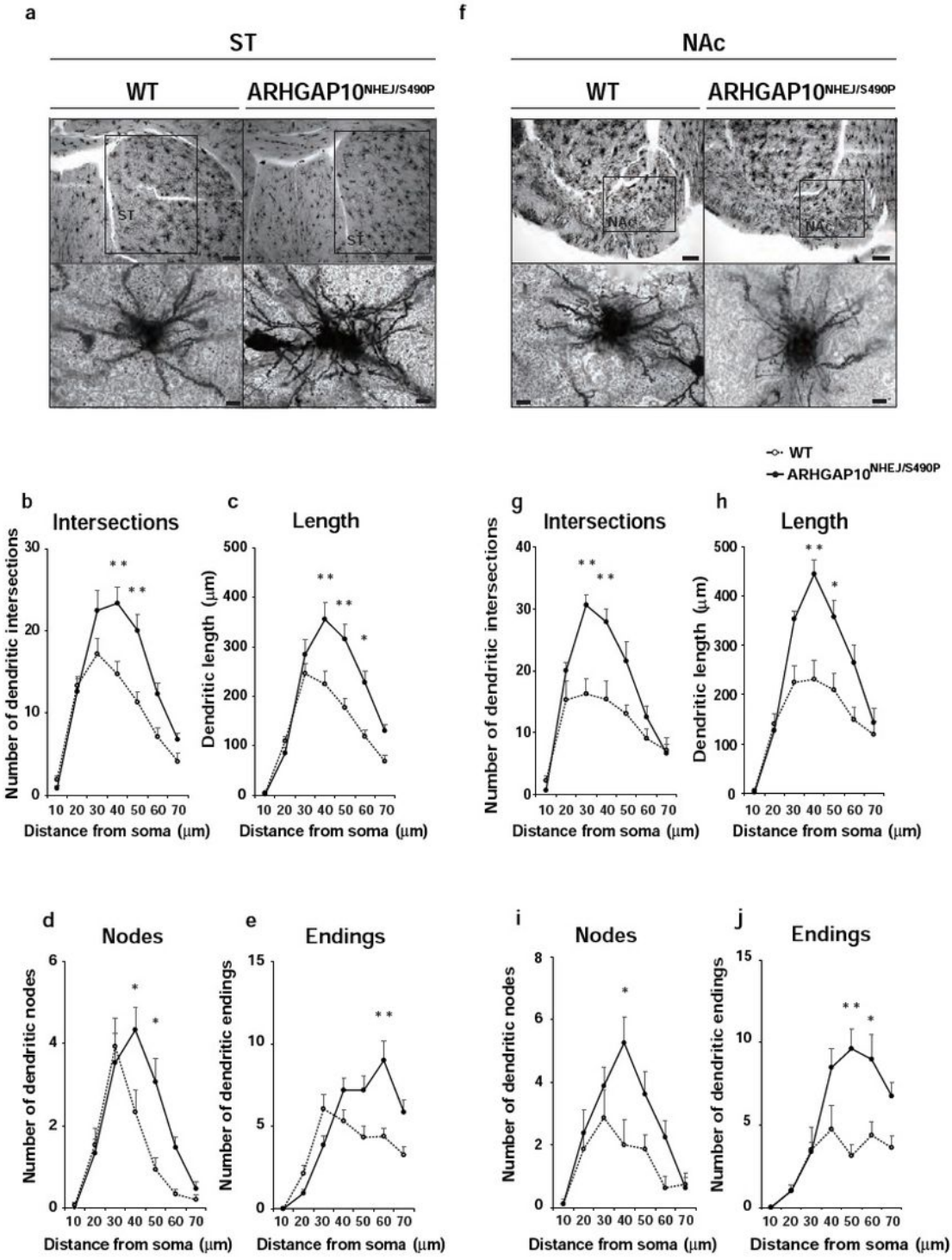

Figure 3

Abnormal neuronal morphology in the ST and NAc of ARHGAP10NHEJ/S490P mice (a, f) Representative images of Golgi-stained single neurons in the ST (a) and NAc (f). Scale bar: upper panel 300 □m and lower panel 10 □m. (b–e, g–j) quantitative analyses of (b, g) intersection, (c, h) length, (d, i) nodes, (e, j) ending in the (b–e) ST and (g–j) NAc. *p < 0.05, ** p < 0.01. All data are expressed as means ± SEM (n = 8–15 neurons from 4–5 mice in each genotype).

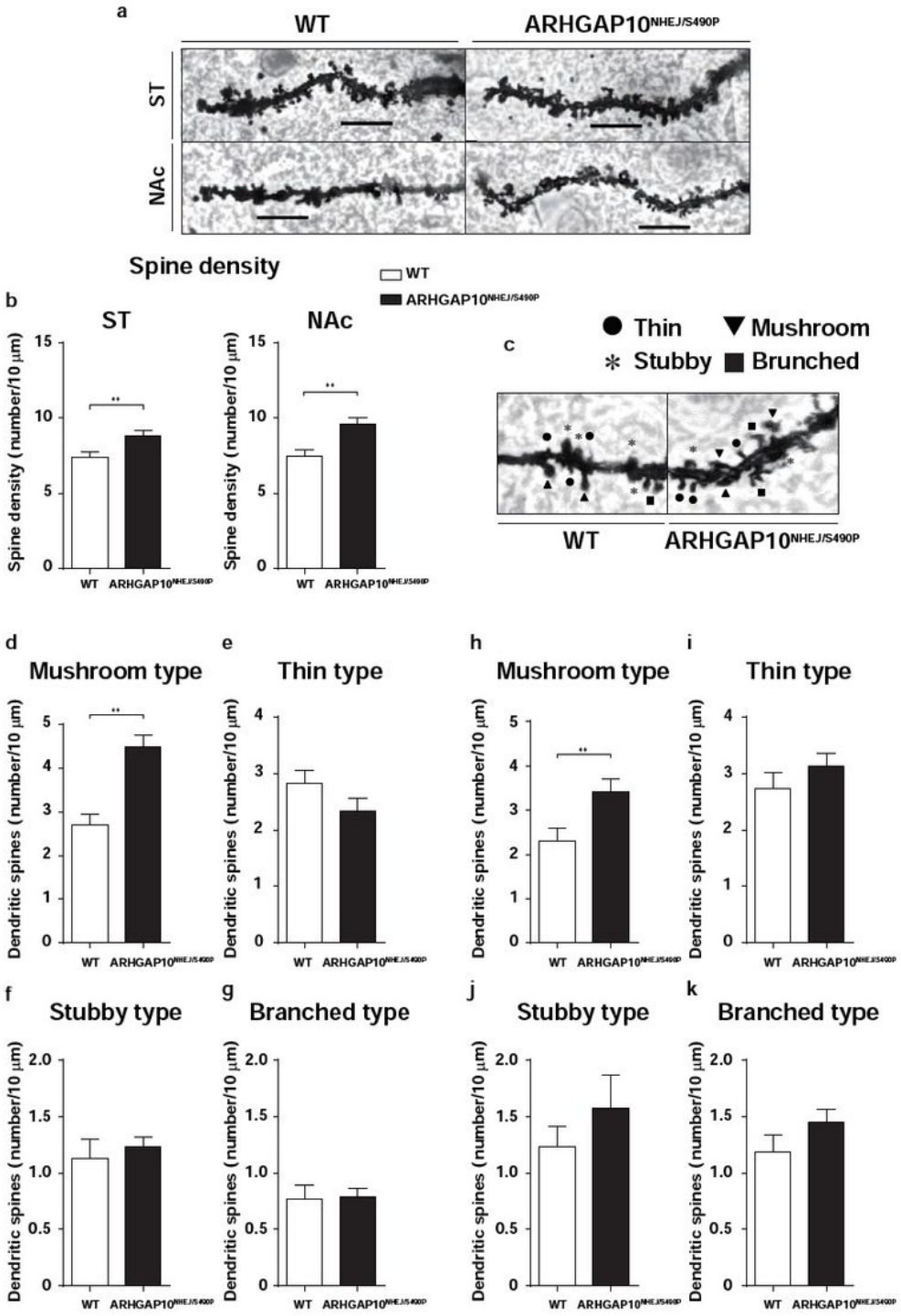

Figure 4

Changes in spine density and morphology in the ST and NAc of ARHGAP10NHEJ/S490P mice (a) Representative images of the ST and NAc dendric spines (Scale bar indicates 10 um). (b) Spine densities of the ST and NAc neurons. (c) Representative images of a dendritic segment illustrating different spine subtypes in NAc. (d–k) Quantification of dendritic spine: (d, h) mushroom, (e, i) thin, (f, j) stubby, and (g, k) brunched types in the (d-g) ST and (h-k) NAc neurons, respectively. ** p < 0.01. All data are expressed as means ± SEM (n = 16 neurons from 4 mice in each genotype).

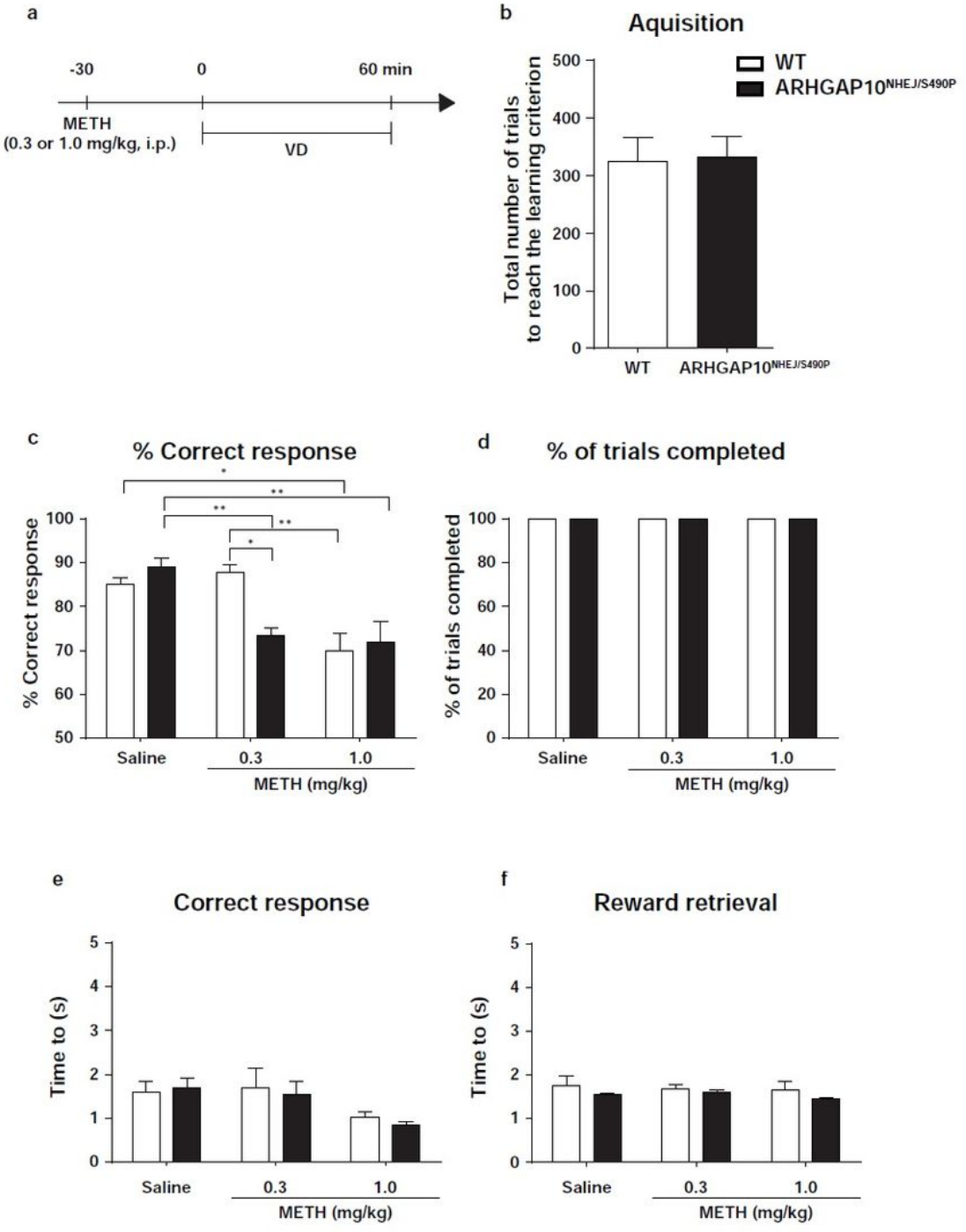

Figure 5

Impairment of VD in ARHGAP10NHEJ/S490P mice induced by METH (a) Mice were administered METH (0.3 or 1.0 mg/kg. i.p.) 30 min before the VD task. (b) Total number of trials to reach the learning criterion in VD task. (c) Percentage of the correct response. (d) Percentage of trials completed. (e) Time to correct response. (f) Time to reward retrieval. *p < 0.05, ** p < 0.01. All data are expressed as means ± SEM (WT mice n = 6, ARHGAP10NHEJ/S490P mice n = 7).

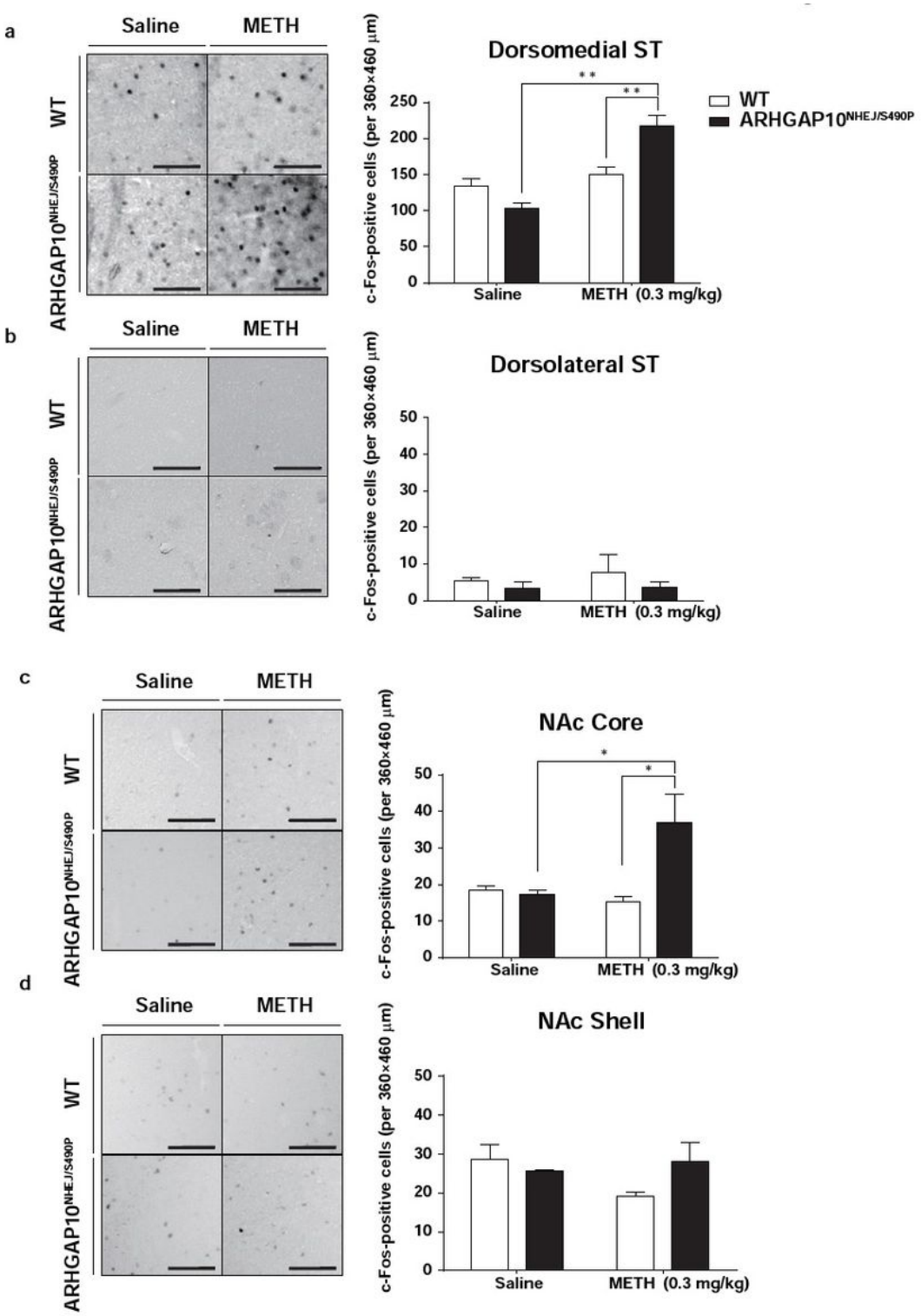

Figure 6

METH-induced changes in neuronal activity of the dorsal ST and NAc in ARHGAP10NHEJ/S490P mice (a-d) Representative images and the number of c-Fos-positive cells in the (a) dorsomedial ST, (b) dorsolateral ST, (c) NAc core and (d) NAc shell. Scale bar indicates 100 □m. *p < 0.05, ** p < 0.01. All data are expressed as means ± SEM (n = 9 slices from 3 mice in each group).

Supplementary Files

This is a list of supplementary files associated with this preprint. Click to download.

- Additionalfile2.pdf
- Additionalfile1.pdf